

# Competitive Oxygen Reduction Pathways to Superoxide and Peroxide during Sodium-Oxygen Battery Discharge

Zarko P. Jovanov,<sup>[a, f]</sup> Lukas Lutz,<sup>[a, b]</sup> Juan G. Lozano,<sup>[a]</sup> Conrad Holc,<sup>[a, c]</sup> Xiangwen Gao,<sup>[a, d]</sup> Alexis Grimaud,<sup>[b]</sup> Jean-Marie Tarascon,<sup>[b]</sup> Yuhui Chen,<sup>\*[e]</sup> Lee R. Johnson,<sup>\*[c]</sup> and Peter G. Bruce<sup>\*[a]</sup>

The sodium-air battery offers a sustainable, high-energy alternative to lithium-ion batteries. Discharge in the cell containing glyme-based electrolytes can lead to formation of large cubic  $\text{NaO}_2$  particles via a solution-precipitation mechanism. While promising, high rates result in sudden death. The exact nature of the discharge product has been a matter of contention, and  $\text{Na}_2\text{O}_2$  has never been directly detected in a dry glyme  $\text{Na}-\text{O}_2$  cell. If  $\text{Na}_2\text{O}_2$  were to form during discharge in the  $\text{Na}-\text{O}_2$  cell it

would have a detrimental impact on cell performance. Here we show that  $\text{Na}_2\text{O}_2$  forms during discharge at high overpotential in the glyme-based  $\text{Na}-\text{O}_2$  batteries.  $\text{Na}_2\text{O}_2$  formation is confirmed by spectroscopic and electrochemical analysis and electron microscopy demonstrates that it results in thin insulating films at the electrode surface. The formation of these thin films results in rapid cell death during discharge, introducing an inherent chemical limitation to the  $\text{Na}-\text{O}_2$  battery.

## Introduction

Metal-air ( $\text{O}_2$ ) batteries are promising high specific energy alternatives to lithium-ion batteries.<sup>[1–11]</sup> In the aprotic sodium-oxygen ( $\text{Na}-\text{O}_2$ ) battery, sodium metal is oxidized on discharge and oxygen is reduced at the positive electrode.<sup>[12–14]</sup> In  $\text{Na}-\text{O}_2$  batteries containing glyme-based electrolytes,  $\text{NaO}_2$  is found to

be the major discharge product and it is commonly reported to form large cubic crystals.<sup>[12,15–17]</sup> The formation of  $\text{NaO}_2$  crystals occurs via the dissolution of  $\text{NaO}_2$  at the electrode surface and its subsequent precipitation away from the electrode. The solubility is controlled in part by the solvent donor number, as is the case in the  $\text{Li}-\text{O}_2$  system,<sup>[18–20]</sup> as well as the  $\text{Na}^+$  activity.<sup>[21]</sup> Several publications have shown promising results with this system.<sup>[4,13,22–24]</sup> Advantages of the  $\text{Na}-\text{O}_2$  battery compared to the  $\text{Li}-\text{O}_2$  battery stem from the formation of a superoxide rather than a peroxide, as this simple electrochemical reaction and soluble product results in relatively low polarisation and higher rates during cycling.<sup>[2,7,25,26]</sup> However, parasitic chemical reactions can occur, impacting on the cyclability of cells. This arises from reactions of both the Na electrode and the  $\text{NaO}_2$  discharge product, but careful selection of electrolytes and cycling parameters can mitigate these issues.<sup>[27,28]</sup>

At high rates, the capacity of typical glyme-based  $\text{Na}-\text{O}_2$  cells is lower and sudden death of the cell is common.<sup>[2,29,30]</sup> This has been linked to the formation of  $\text{NaO}_2$  thin films at the electrode surface.<sup>[20,29]</sup> We have shown that this is in part due to the limited solubility and rate of (de)solvation of  $\text{NaO}_2$ ,<sup>[31]</sup> which must be rapid enough to sustain the dissolution-precipitation mechanism by which  $\text{NaO}_2$  cubes grow.<sup>[20,29]</sup> However, computational studies have shown that electrochemical formation of  $\text{Na}_2\text{O}_2$  may also be possible at higher overpotentials.<sup>[15]</sup> It is well known that in the  $\text{Li}-\text{O}_2$  cell,  $\text{O}_2$  is reduced to  $\text{Li}_2\text{O}_2$ , which is more stable than  $\text{LiO}_2$ .<sup>[19,32–35]</sup> Unlike the  $\text{Li}-\text{O}_2$  system, the theoretical equilibrium potentials for the formation of  $\text{NaO}_2$  and  $\text{Na}_2\text{O}_2$  from oxygen are only 60 mV apart (2.27 V for  $\text{NaO}_2$  and 2.33 V for  $\text{Na}_2\text{O}_2$  vs.  $\text{Na}/\text{Na}^+$ ). If  $\text{Na}_2\text{O}_2$  were to form during discharge in the  $\text{Na}-\text{O}_2$  cell it would have a detrimental impact on cell performance and remove many of its advantages over the  $\text{Li}-\text{O}_2$  battery. The discharge product(s) and performance of  $\text{Na}-\text{O}_2$  cells are influenced by several factors, including electro-

[a] Dr. Z. P. Jovanov, Dr. L. Lutz, Dr. J. G. Lozano, Dr. C. Holc, Dr. X. Gao, Prof. P. G. Bruce

Departments of Materials and Chemistry, University of Oxford  
Oxford, OX2 6HT, U.K.

E-mail: peter.bruce@materials.ox.ac.uk

[b] Dr. L. Lutz, Dr. A. Grimaud, Prof. J.-M. Tarascon  
Collège de France  
11 place Marcelin Berthelot, 75231 Paris Cedex, France

[c] Dr. C. Holc, Dr. L. R. Johnson  
Nottingham Applied Materials and Interfaces (NAMI),  
Group GSK Carbon Neutral Laboratories for Sustainable Chemistry,  
University of Nottingham

Nottingham, NG7 2TU, U.K.  
E-mail: Lee.johnson@nottingham.ac.uk

[d] Dr. X. Gao  
Materials Science and Engineering Program and Texas Materials Institute,  
The University of Texas at Austin  
Austin, TX 78712, U.S.A.

[e] Prof. Y. Chen  
State Key Laboratory of Materials-oriented Chemical Engineering,  
College of Chemical Engineering and  
School of Energy Science and Engineering,  
Nanjing Tech University Nanjing  
Jiangsu, 211816, China  
E-mail: cheny@njtech.edu.cn

[f] Dr. Z. P. Jovanov  
LIQUIDLOOP GmbH  
Hardenbergstr. 38, 10623 Berlin, Germany

 Supporting information for this article is available on the WWW under  
<https://doi.org/10.1002/batt.202200055>

 © 2022 The Authors. *Batteries & Supercaps* published by Wiley-VCH GmbH.  
This is an open access article under the terms of the Creative Commons  
Attribution License, which permits use, distribution and reproduction in any  
medium, provided the original work is properly cited.

lyte composition and the nature of the electrode surface.<sup>[12,31,36]</sup> Na<sub>2</sub>O<sub>2</sub> has been observed in the cell with acetonitrile and NaO<sub>2</sub> has been shown to disproportionate to Na<sub>2</sub>O<sub>2</sub> in this solvent.<sup>[37]</sup> This is ascribed to the low donor number of acetonitrile. Attempts have been made to form Na<sub>2</sub>O<sub>2</sub> in other electrolytes, but these require conditions which enhance the surface binding of NaO<sub>2</sub>, such as the use of Au electrodes, in conjunction with high overpotentials.<sup>[38]</sup> Some Pt facets and Cu nanoparticles have also been shown to favour Na<sub>2</sub>O<sub>2</sub> formation on discharge.<sup>[39,40]</sup> Na<sub>2</sub>O<sub>2</sub> has been observed when discharging at high overpotential at a TEM grid, noting that this contains both carbon and gold.<sup>[41]</sup> Hydrated peroxide (Na<sub>2</sub>O<sub>2</sub>·H<sub>2</sub>O) and NaOH have been reported in glyme-based electrolytes due to contamination of the system with water from sources including the O<sub>2</sub> gas supply and electrolyte.<sup>[14,42]</sup> Although, trace quantities of water have also been shown to promote NaO<sub>2</sub> solution growth via phase-transfer catalysis.<sup>[43]</sup> During standard cycling conditions (dry electrolyte with a carbon electrode), it is generally assumed that Na<sub>2</sub>O<sub>2</sub> does not form during discharge in the Na–O<sub>2</sub> cell containing glyme ethers.

Here we explore the impact of overpotential on the electrochemical reduction of oxygen in the glyme-based Na–O<sub>2</sub> batteries and the role this plays in product selection, NaO<sub>2</sub> versus Na<sub>2</sub>O<sub>2</sub>, and cell performance. The capacity is measured

at various rates and as is the distribution, morphology, and chemistry of the discharged product at the positive electrode. Electrochemical analysis is used to propose discharge routes that explain these observations. The formation of thin Na<sub>2</sub>O<sub>2</sub> films is conclusively demonstrated and shown to be detrimental to cell performance.

## Results and Discussion

### Impact of discharge rate on the capacity of the sodium–O<sub>2</sub> battery

To explore the impact of discharge rate, and thus overpotential, on the discharge product and capacity of the Na–O<sub>2</sub> battery, a series of Swagelok-type Na–O<sub>2</sub> cells were discharged at three different current densities: 0.025, 0.25 and 0.4 mA cm<sup>-2</sup>. The electrolyte was 0.5 M sodium triflate (NaOTf) in diethylene glycol dimethyl ether (DEGDME) and the electrode was carbon, consistent with state-of-the-art cells.<sup>[31]</sup> Figure 1(a) shows the discharge profiles collected from the Na–O<sub>2</sub> cells. At a lower current density of 0.025 mA cm<sup>-2</sup>, the battery achieved a relatively large discharge capacity of over 4 mAh cm<sup>-2</sup>, which is typical for an Na–O<sub>2</sub> cell. The dominant formation of NaO<sub>2</sub>

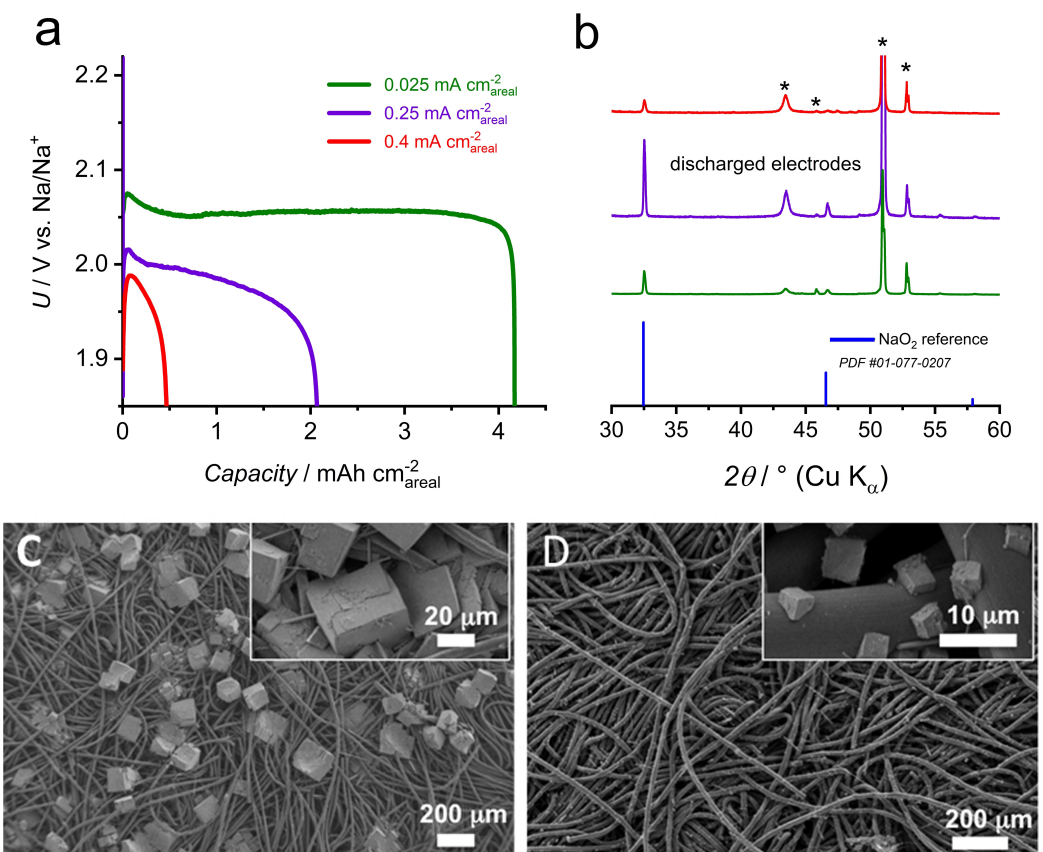


**Figure 1.** Discharge performance of Na–O<sub>2</sub> (Swagelok) cells: a) discharge profiles at three different current densities using O<sub>2</sub> saturated 0.5 M NaOTf in DEGDME; b) the corresponding PXRD patterns of the discharge positive electrodes. Three current densities are used: 0.025 mA cm<sup>-2</sup> (green line), 0.25 mA cm<sup>-2</sup> (purple line) and 0.4 mA cm<sup>-2</sup> (red line). Peaks marked with a black asterisk (\*) correspond to the sample holder and GDL. SEM images of the positive electrode after discharge at c) 0.025 mA cm<sup>-2</sup> and d) 0.4 mA cm<sup>-2</sup>.

confirmed by powder X-ray diffraction (PXRD), Figure 1(b). Figure 1(c) shows an SEM image of the discharged positive electrode showing numerous large cube-shaped structures, consistent with the dominant formation of  $\text{NaO}_2$  by a solution precipitation mechanism.<sup>[2,13,20]</sup> Upon increasing the current density to move to practical values, the voltage of the discharge plateaus shifted negative, discharge capacities decreased dramatically, and the cell death (rapid negative shift in voltage) rapidly occurred, Figure 1(a). This is also accompanied by an initial drop in potential, which we suggest is associated with the nucleation barrier for formation of  $\text{NaO}_2$  on the carbon surface, Figure S1. SEM images, Figure 1(d), showed that the  $\text{NaO}_2$  cubes became smaller and fewer in number at a higher current density. Previous studies have shown that current density has an impact on  $\text{NaO}_2$  particle size.<sup>[20,31,44]</sup> PXRD indicates that the only product is  $\text{NaO}_2$ , Figure 1(b). Interestingly, cubic  $\text{NaO}_2$  does not completely cover the electrode surface and large areas of apparent bare carbon remain. Passivation of the electrode surface by  $\text{NaO}_2$  cubes at high rates cannot explain cell death.

#### Soluble versus surface-grown discharge products

To investigate the electrochemistry of oxygen reduction in  $\text{Na}^+$ -ion-containing DEGDME in more detail, we employed a rotating ring-disk electrode (RRDE), Figure 2. Oxygen is reduced at the

rotating disk electrode ( $i_{\text{disk}}$ ), while any soluble  $\text{O}_2^-$  formed is detected at a ring electrode ( $i_{\text{ring}}$ ) by holding it at an oxidising potential (3.7 V vs.  $\text{Na}/\text{Na}^+$ ). The difference between the ring and the disk current can be assigned to insoluble products ( $i_{\text{surface}}$ ), e.g.,  $\text{NaO}_{2(\text{s})}$ ,  $\text{Na}_2\text{O}_{2(\text{s})}$ , and can be used to identify the electrochemical potential at which a second reduction reaction occurs.  $\text{NaO}_2$  does not disproportionate to form  $\text{Na}_2\text{O}_2$  in  $\text{Na}^+$ -ion containing DEGDME and therefore only electrochemical routes need to be considered.<sup>[37]</sup> The disk current rapidly increases between 2.5 V and 2.0 V vs.  $\text{Na}/\text{Na}^+$ . At low overpotentials,  $i_{\text{disk}}$  mirrors  $i_{\text{ring}}$ , indicating that the reaction is almost exclusively forming dissolved  $\text{O}_2^-$ , rather than solid  $\text{NaO}_2$ . At higher overpotentials,  $i_{\text{ring}}$  no longer fully accounts for  $i_{\text{disk}}$ , and this coincides with a peak in the current followed by a drop to zero current, demonstrating passivation of the electrode surface by the discharge product. The potential at which this occurs mirrors the sudden death potential of the  $\text{Na}-\text{O}_2$  cells and indicates that it is responsible for the limited capacity seen at high overpotentials.

#### Surface confined discharge products in the sodium- $\text{O}_2$ battery

To identify the nature of the passivating film,  $\text{Na}-\text{O}_2$  cells were constructed using carbon nanofiber as the electrode (prepared as described in the Supporting Information), which are suitable

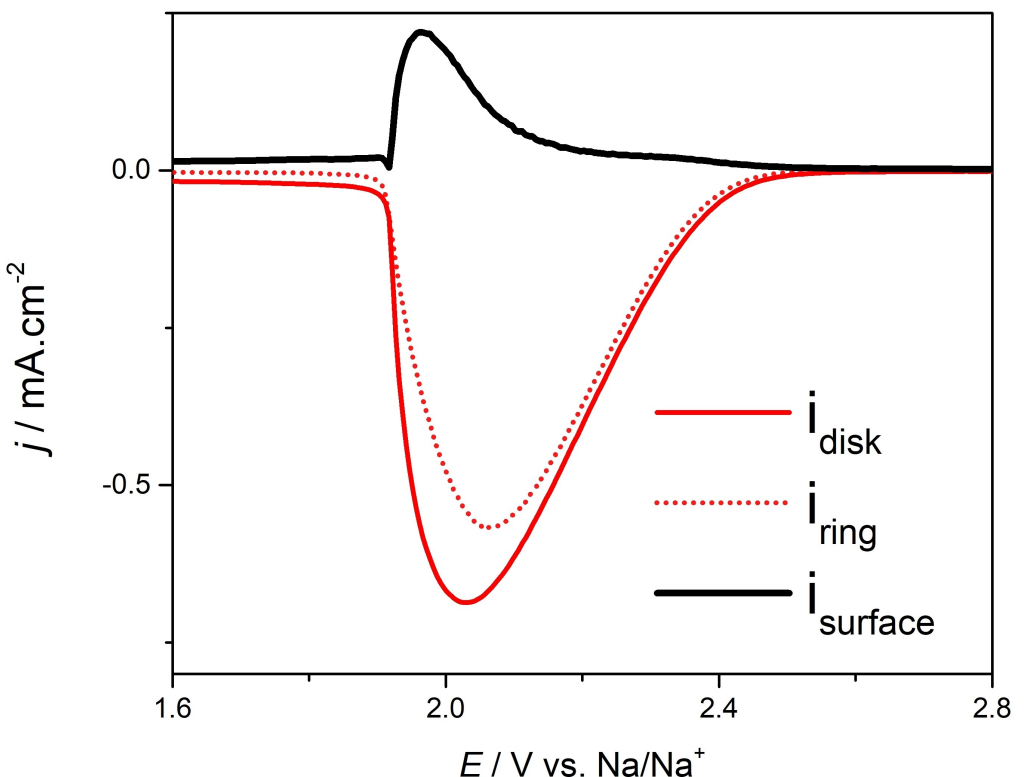


**Figure 2.** RRDE voltammetry in  $\text{O}_2$  saturated 0.5 M  $\text{NaOTf}$  in DEGDME. Measurements were recorded at Au disk-Au ring electrode at a scan rate of  $20 \text{ mV s}^{-1}$  and a rotation speed of 2000 rpm.  $i_{\text{disk}}$  (red solid line) is the overall current measured,  $i_{\text{ring}}$  (red dashed line) is the current due to the formation of soluble species and  $i_{\text{surface}}$  (black solid line) is the difference between the two which is assigned to insoluble species.

for use in high resolution transmission electron microscopy (HRTEM) measurements, such that it is possible to observe any nanometer thick discharge products that form at the electrode. The cells were discharged in O<sub>2</sub>-saturated 0.25 M NaOTf in DEGDME at a high current density (0.4 mA cm<sup>-2</sup>) resulting in an overpotential of approximately 500 mV and the surface was analyzed using HRTEM, Figure 3. The images unambiguously demonstrate the formation of a 20–30 nm thick film of discharge product at the electrode surface. Previously it has been proposed that surface films of NaO<sub>2</sub> are responsible for sudden death at high discharge rates.<sup>[29]</sup> This is a reasonable conclusion as neither PXRD nor X-ray photoelectron spectroscopy (XPS) analysis typically identifies Na<sub>2</sub>O<sub>2</sub> in discharged electrodes. However, previous analyses of the Li<sup>+</sup>-ion containing system have shown that electrochemically formed peroxide is non-crystalline, explaining why Na<sub>2</sub>O<sub>2</sub> may not be detected by PXRD.<sup>[45]</sup> In addition, examination of SEM images, Figure 1, shows that NaO<sub>2</sub> cubes are the major discharge product in all cases making detection of trace Na<sub>2</sub>O<sub>2</sub> difficult. Here we perform XPS analysis on a positive electrode discharged at a constant potential of 1.9 V vs. Na/Na<sup>+</sup>, where sudden death of the cell occurs. A flooded cell containing large volumes of electrolyte was used, such that much of the NaO<sub>2</sub> is dissolved and the relative signal for any insoluble products (i.e., Na<sub>2</sub>O<sub>2</sub>) is enhanced. The oxygen 1 s region of the resulting spectrum is shown in Figure 3(c). The spectrum displayed a major peak centred at 530.9 eV, confirming the formation of peroxide during discharge at high overpotential.<sup>[7,46]</sup> No peak consistent with the formation of Na<sub>2</sub>O (529.7 eV) was observed.<sup>[47]</sup> The peak centred at 532.9 eV is due to the formation of superoxide and appears to make up a minor contribution to the overall XPS signal.<sup>[7]</sup> However, we reiterate that in a real cell with low electrolyte volume where NaO<sub>2</sub> is trapped in the electrode structure, NaO<sub>2</sub> is the major product, Figure S2, but only small amounts of Na<sub>2</sub>O<sub>2</sub> are needed to have a detrimental impact on performance.

The data demonstrates the occurrence of two reaction processes, one at lower overpotential, which results in a soluble superoxide product and the formation of the anticipated NaO<sub>2</sub> cubes, and a second at a larger overpotential that results in the formation of passivating films of product that cover the electrode surface. The results are consistent with a 1e<sup>-</sup> reduction of O<sub>2</sub> to soluble O<sub>2</sub><sup>-</sup> stabilised by alkali ions in the solvation shell, followed by a second reduction step to Na<sub>2</sub>O<sub>2</sub>, Equations (1 and 2);



Onset of this second reduction will inevitably result in rapid electrode passivation and cell death and explains the trend seen during discharge of Na-O<sub>2</sub> cells at varying rates. These results suggest that Na<sub>2</sub>O<sub>2</sub> formation is unavoidable at high overpotential presenting a challenge for the development of high-rate Na-O<sub>2</sub> batteries. Moreover, trace amount of Na<sub>2</sub>O<sub>2</sub> could accumulate during cycling and its removal will likely

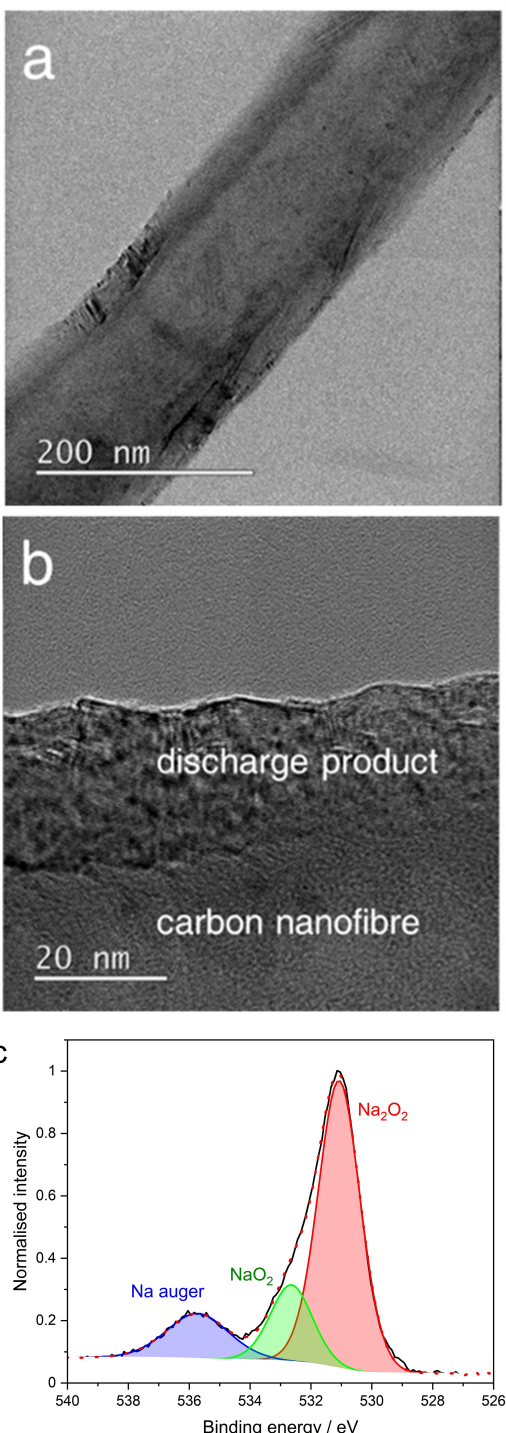


**Figure 3.** HRTEM images and spectroscopic analysis of the thin film product formed at the positive electrode of the Na-O<sub>2</sub> battery: a and b) HRTEM images showing the film deposited on carbon nanofiber electrodes during discharge at high rates (0.4 mA cm<sup>-2</sup>). c) X-ray photoelectron spectra in the O 1s region of Na-O<sub>2</sub> positive electrodes discharged at a constant potential of 1.9 V vs. Na/Na<sup>+</sup>. The peaks at 530.9 eV, 532.9 eV and 536 eV are due to Na<sub>2</sub>O<sub>2</sub>, NaO<sub>2</sub> and the Na auger response, respectively.

require high overpotentials during charging, eliminating many of the advantages of the Na-O<sub>2</sub> battery over the Li-O<sub>2</sub> battery. We note that changing the electrolyte solution or electrode

material would alter the potential at which  $\text{Na}_2\text{O}_2$  forms and this could be a route to avoid its detrimental impact.

## Conclusion

Here we show that the product of the aprotic oxygen reduction with  $\text{Na}^+$  ions in glyme ethers depends on the overpotential during discharge. At low overpotential, the reaction forms the  $1\text{e}^-$  reduction product  $\text{NaO}_2$ , which is soluble in glyme-based electrolyte and results in the formation of cubic  $\text{NaO}_2$  structures in the electrode and high capacities. At high overpotential, the reaction switches to a  $2\text{e}^-$  reduction, which forms thin films of passivating  $\text{Na}_2\text{O}_2$  across the surface of the electrode. If high rates are allowed to significantly polarise the voltage of  $\text{Na}-\text{O}_2$  cells, the formation of  $\text{Na}_2\text{O}_2$  passivating layers result in capacity limitation and rapid cell failure. To achieve high capacity and high rates, processes that result in polarisation of the electrode potential must be minimised. Practical cells will require high rates of electrochemical reduction of oxygen, together with rapid nucleation and growth of  $\text{NaO}_2$ , and high mass-transport of oxygen and  $\text{Na}^+$  ions, thus avoiding voltage polarisation and detrimental  $\text{Na}_2\text{O}_2$  formation.

## Experimental Section

### Materials and Methods

Diethylene glycol dimethyl ether (Diglyme or DEGDME) was distilled under argon over  $\text{CaH}_2$ . The solvent was further dried for several days over freshly activated molecular sieves (type 4 Å). The final water content was  $\leq 4$  ppm (determined by Karl Fischer titration). Tetrabutylammonium trifluorosulfonate/triflate (TBAOTf) was recrystallised from a mixture of dichloromethane and diethyl ether and then dried under vacuum at  $80^\circ\text{C}$  for 3 days. Sodium triflate ( $\text{NaOTf}$ ) was recrystallised from a mixture of dimethyl sulfoxide (DMSO) and dichloromethane and then dried under vacuum at  $80^\circ\text{C}$  for 3 days. All materials were stored in an argon glove box. High purity N5  $\text{O}_2$  was obtained from BOC industrial gases and was used in all measurements. During measurements,  $\text{O}_2$  was passed through a drying column consisting of freshly activated molecular sieves before entering the cell. Bubbling  $\text{O}_2$  into the electrolyte solution for 10 mins did not change the electrolyte water content.

### Electrochemical Analysis

Electrochemical measurements were performed using a VMP3 electrochemical workstation (Biologic) and a multi-necked, air-tight glass cell within a glove box. Electrochemical measurements were carried out at room temperature and IR correction was used. 3 mm diameter polycrystalline Au disks (BAS Inc.) were employed as the working electrodes. Prior to use, the working electrodes were polished in a glove box with  $0.05\ \mu\text{m}$  alumina slurry in ethanol and rinsed with copious amounts of ethanol followed by drying under vacuum. Platinum wire served as the counter electrode. Measurements were performed using a reference electrode based on  $\text{LiFePO}_4$ . It was first pre-oxidized (20% of total capacity) to  $\text{Li}_x\text{FePO}_4$ , which has a constant potential. This is then placed in 0.1 M  $\text{LiClO}_4$  in DMSO separated from the bulk electrolyte with a porous frit,

thus providing a fixed potential. Potentials were corrected to  $\text{Na}/\text{Na}^+$  using an internal ferrocene reference and by subtracting 3.6 V. Electrolytes were saturated with  $\text{O}_2$ . Carbon nanofibre electrodes were formed from a nanofiber, PTFE suspension in isopropanol which was cast onto stainless steel mesh, dried under vacuum, and discharged at constant current in a three-electrode cell. Rotating ring/disk electrode, RRDE, measurements were performed using a MSR rotator and a removable disk rotating ring/disk electrode containing an Au disk (5 mm diameter) and a glassy carbon ring (PINE instruments). A ring potential of 3.7 V vs.  $\text{Na}/\text{Na}^+$  was used. Measurements were performed in a glove box in a round bottom flask and all necks other than the neck containing the shaft were sealed. The electrode was polished as described above between measurements. The collection efficiency at the ring,  $N$ , in each experiment was determined using an ideal redox couple.

$\text{Na}-\text{O}_2$  cells were built from a modified Swagelok setup. The cell was vacuum-dried under elevated temperature and transferred into a glovebox (0.1 ppm  $\text{H}_2\text{O}$ , 0.1 ppm  $\text{O}_2$ ). The anode was made from metallic sodium (Sigma-Aldrich), cut into a  $0.5\ \text{cm}^2$  disc. 0.3 mL Dried electrolyte solution (0.5 M sodium salt in diglyme) was imbibed on two Whatman glass fibre filters (QM-A grade) (dried under vacuum at  $260^\circ\text{C}$ , 24 h). A piece of GDL ( $1.13\ \text{cm}^2$  of surface area,  $210\ \mu\text{m}$  in thickness, and a weight of 10 mg) was used as cathode and held by an inox mesh current collector containing holes for gas exchange. No further insulating sleeve was used. The assembled cells were transferred from the glovebox to a filling station, and after a first evacuating step, the cells were pressurized with dry, ultrapure  $\text{O}_2$  to 1.3 bar. To guarantee stable temperature conditions, the cells were mounted inside of a temperature-controlled incubator ( $25.0 \pm 0.1^\circ\text{C}$ ). The electrochemical measurements were performed under temperature-controlled conditions ( $25.0^\circ\text{C}$ ) after resting for 4 h at the open-circuit voltage and using a Bio-Logic VMP3 potentiostat.

### Characterization

X-ray photoelectron spectroscopy was performed on a Thermo Scientific K-Alpha X-ray photoelectron spectrometer (XPS) instrument equipped with a microfocussed monochromated Al X-ray source. The source was operated at 12 keV and a 400 micron spot size was used. The analyser operates at a constant analyser energy (CAE) 200 eV for survey scans and 50 eV for detailed scans. Charge neutralization was applied using a combined low energy/ion flood source. Powder X-ray diffraction (PXRD) measurements were performed by washing samples with dried diglyme prior to PXRD analysis. A Bruker D8 Advance diffractometer with a  $\text{Cu K}_\alpha$  radiation source ( $\lambda_1 = 1.5405\ \text{\AA}$ ,  $\lambda_2 = 1.5443\ \text{\AA}$ ) and a LynxEye XE detector was used to collect the PXRD patterns. The PXRD patterns were recorded for 30 min in the  $2\theta$  range of  $20^\circ$ – $65^\circ$ . A special airtight cell with a beryllium window was used to guarantee no ambient air contamination during PXRD measurements.

### Acknowledgements

P.G.B. is indebted to the EPSRC including the SUPERGEN program for financial support. L.R.J. gratefully acknowledges support from the University of Nottingham's Beacon in Propulsion Futures and the EPSRC (EP/S001611/1).

## Conflict of Interest

The authors declare no conflict of interest.

## Data Availability Statement

The data that support the findings of this study are available from the corresponding authors upon reasonable request.

**Keywords:** diglyme · oxygen reduction reaction · passivating films · sodium peroxide · sodium superoxide

- [1] X. Gao, Y. Chen, L. R. Johnson, Z. P. Jovanov, P. G. Bruce, *Nat. Energy* **2017**, *2*, 17118.
- [2] P. Hartmann, C. L. Bender, M. Vracar, A. K. Duerr, A. Garsuch, J. Janeck, P. Adelhelm, *Nat. Mater.* **2013**, *12*, 228–232.
- [3] Z. Pan, Y. Chen, F. Li, T. Zhang, C. Liu, H. Zhou, *J. Power Sources* **2014**, *251*, 466–469.
- [4] Q. Sun, H. Yadegari, M. N. Banis, J. Liu, B. Xiao, X. Li, C. Langford, R. Li, X. Sun, *J. Phys. Chem. C* **2015**, *119*, 13433–13441.
- [5] C. Xia, C. Y. Kwok, L. F. Nazar, *Science* **2018**, *361*, 777–781.
- [6] D. Aurbach, B. D. McCloskey, L. F. Nazar, P. G. Bruce, *Nat. Energy* **2016**, *1*, 16128.
- [7] J.-H. Kang, W.-J. Kwak, D. Aurbach, Y.-K. Sun, *J. Mater. Chem. A* **2017**, *5*, 20678–20686.
- [8] G. Cong, W. Wang, N.-C. Lai, Z. Liang, Y.-C. Lu, *Nat. Mater.* **2019**, *18*, 390–396.
- [9] J. Lu, Y. J. Lee, X. Luo, K. C. Lau, M. Asadi, H.-H. Wang, S. Brombosz, J. Wen, D. Zhai, Z. Chen, D. J. Miller, Y. S. Jeong, J.-B. Park, Z. Z. Fang, B. Kumar, A. Salehi-Khojin, Y.-K. Sun, L. A. Curtiss, K. Amine, *Nature* **2016**, *529*, 377–382.
- [10] Y. Chen, Z. P. Jovanov, X. Gao, J. Liu, C. Holc, L. R. Johnson, P. G. Bruce, *J. Electroanal. Chem.* **2018**, *819*, 542–546.
- [11] M. Balaish, X. Gao, P. G. Bruce, Y. Ein-Eli, *Adv. Mater.* **2019**, *4*, 1800645.
- [12] C. L. Bender, D. Schroder, R. Pinedo, P. Adelhelm, J. Janeck, *Angew. Chem. Int. Ed.* **2016**, *55*, 4640–4649; *Angew. Chem.* **2016**, *128*, 4716–4726.
- [13] P. Hartmann, M. Heinemann, C. L. Bender, K. Graf, R.-P. Baumann, P. Adelhelm, C. Heiliger, J. Janeck, *J. Phys. Chem. C* **2015**, *119*, 22778–22786.
- [14] R. Pinedo, D. A. Weber, B. Bergner, D. Schröder, P. Adelhelm, J. Janeck, *J. Phys. Chem. C* **2016**, *120*, 8472–8481.
- [15] D. Krishnamurthy, H. A. Hansen, V. Viswanathan, *ACS Energy Lett.* **2016**, *1*, 162–168.
- [16] I. I. Abate, L. E. Thompson, H.-C. Kim, N. B. Aetukuri, *J. Phys. Chem. Lett.* **2016**, *7*, 2164–2169.
- [17] C. J. Allen, J. Hwang, R. Kautz, S. Mukerjee, E. J. Plichta, M. A. Hendrickson, K. M. Abraham, *J. Phys. Chem. C* **2012**, *116*, 20755–20764.
- [18] I. M. Aldous, L. J. Hardwick, *Angew. Chem. Int. Ed.* **2016**, *55*, 8254–8257; *Angew. Chem.* **2016**, *128*, 8394–8397.
- [19] L. Johnson, C. Li, Z. Liu, Y. Chen, S. A. Freunberger, P. C. Ashok, B. B. Praveen, K. Dholakia, J.-M. Tarascon, P. G. Bruce, *Nat. Chem.* **2014**, *6*, 1091–1099.
- [20] L. Lutz, W. Yin, A. Grimaud, D. Alves Dalla Corte, M. Tang, L. Johnson, E. Azaceta, V. Sarou-Kanian, A. J. Naylor, S. Hamad, J. A. Anta, E. Salager, R. Tena-Zaera, P. G. Bruce, J. M. Tarascon, *J. Phys. Chem. C* **2016**, *120*, 20068–20076.
- [21] R. Tatara, G. M. Leverick, S. Feng, S. Wan, S. Terada, K. Dokko, M. Watanabe, Y. Shao-Horn, *J. Phys. Chem. C* **2018**, *122*, 18316–18328.
- [22] S. Kang, Y. Mo, S. P. Ong, G. Ceder, *Nano Lett.* **2014**, *14*, 1016–1020.
- [23] B. Lee, D.-H. Seo, H.-D. Lim, I. Park, K.-Y. Park, J. Kim, K. Kang, *Chem. Mater.* **2014**, *26*, 1048–1055.
- [24] S. Yang, D. J. Siegel, *Chem. Mater.* **2015**, *27*, 3852–3860.
- [25] B. D. McCloskey, J. M. Garcia, A. C. Luntz, *J. Phys. Chem. Lett.* **2014**, *5*, 1230–1235.
- [26] C. L. Bender, P. Hartmann, M. Vračar, P. Adelhelm, J. Janeck, *Adv. Energy Mater.* **2014**, *4*, 1301863.
- [27] S. Y. Sayed, K. P. C. Yao, D. G. Kwabi, T. P. Batcho, C. V. Amanchukwu, S. Feng, C. V. Thompson, Y. Shao-Horn, *Chem. Commun.* **2016**, *52*, 9691–9694.
- [28] L. Lutz, D. Alves Dalla Corte, M. Tang, E. Salager, M. Deschamps, A. Grimaud, L. Johnson, P. G. Bruce, J.-M. Tarascon, *Chem. Mater.* **2017**, *29*, 6066–6075.
- [29] J. E. Nichols, B. D. McCloskey, *J. Phys. Chem. C* **2017**, *121*, 85–96.
- [30] Y. Li, H. Yadegari, X. Li, M. N. Banis, R. Li, X. Sun, *Chem. Commun.* **2013**, *49*, 11731–11733.
- [31] L. Lutz, D. A. D. Corte, Y. Chen, D. Batuk, L. R. Johnson, A. Abakumov, L. Yate, E. Azaceta, P. G. Bruce, J.-M. Tarascon, A. Grimaud, *Adv. Energy Mater.* **2018**, *8*, 1701581.
- [32] M. J. Trahan, I. Gunasekara, S. Mukerjee, E. J. Plichta, M. A. Hendrickson, K. M. Abraham, *J. Electrochem. Soc.* **2014**, *161*, A1706–A1715.
- [33] C. M. Burke, V. Pande, A. Khetan, V. Viswanathan, B. D. McCloskey, *Proc. Natl. Acad. Sci. USA* **2015**, *112*, 9293–9298.
- [34] B. D. Adams, C. Radtke, R. Black, M. L. Trudeau, K. Zaghib, L. F. Nazar, *Energy Environ. Sci.* **2013**, *6*, 1772–1778.
- [35] B. Horstmann, B. Gallant, R. Mitchell, W. G. Bessler, Y. Shao-Horn, M. Z. Bazant, *J. Phys. Chem. Lett.* **2013**, *4*, 4217–4222.
- [36] Z. Zheng, C. Wu, Q. Gu, K. Konstantinov, J. Wang, *Energy Environ. Mater.* **2021**, *4*, 158–177.
- [37] C. Sheng, F. Yu, Y. Wu, Z. Peng, Y. Chen, *Angew. Chem. Int. Ed.* **2018**, *57*, 9906–9910; *Angew. Chem.* **2018**, *130*, 10054–10058.
- [38] S. Ma, W. C. McKee, J. Wang, L. Guo, M. Jansen, Y. Xu, Z. Peng, *Phys. Chem. Chem. Phys.* **2017**, *19*, 12375–12383.
- [39] T. A. Galloway, J.-C. Dong, J.-F. Li, G. Attard, L. J. Hardwick, *Chem. Sci.* **2019**, *10*, 2956–2964.
- [40] S. Han, C. Cai, F. Yang, Y. Zhu, Q. Sun, Y. G. Zhu, H. Li, H. Wang, Y. Shao-Horn, X. Sun, M. Gu, *ACS Nano* **2020**, *14*, 3669–3677.
- [41] I. Landa-Medrano, A. Sorrentino, L. Stievano, I. Ruiz de Laramendi, E. Pereiro, L. Lezama, T. Rojo, D. Toni, *Nano Energy* **2017**, *37*, 224–231.
- [42] C. Liu, M. Carboni, W. R. Brant, R. Pan, J. Hedman, J. Zhu, T. Gustafsson, R. Younesi, *ACS Appl. Mater. Interfaces* **2018**, *10*, 13534–13541.
- [43] C. Xia, R. Black, R. Fernandes, B. Adams, L. F. Nazar, *Nat. Chem.* **2015**, *7*, 496–501.
- [44] N. Ortiz-Vitoriano, T. P. Batcho, D. G. Kwabi, B. Han, N. Pour, K. P. C. Yao, C. V. Thompson, Y. Shao-Horn, *J. Phys. Chem. Lett.* **2015**, *6*, 2636–2643.
- [45] K. U. Schwenke, M. Metzger, T. Restle, M. Piana, H. A. Gasteiger, *J. Electrochem. Soc.* **2015**, *162*, A573–A584.
- [46] H. Yadegari, Y. Li, M. N. Banis, X. Li, B. Wang, Q. Sun, R. Li, T.-K. Sham, X. Cui, X. Sun, *Energy Environ. Sci.* **2014**, *7*, 3747–3757.
- [47] A. Barrie, F. J. Street, *J. Electron Spectrosc. Relat. Phenom.* **1975**, *7*, 1–31.

Manuscript received: January 31, 2022

Revised manuscript received: April 14, 2022

Accepted manuscript online: May 10, 2022

Version of record online: June 15, 2022